Available online at www.sciencedirect.com
SCIENCE DIRECT®
Journal of Sound and Vibration 271 (2004) 705–724
JOURNAL OF SOUND AND VIBRATION
www.elsevier.com/locate/jsvi

Suppressing or inducing chaos in a model of robot arms and mechanical manipulators

Hongjun Cao[a,*], Xuebin Chi[a], Guanrong Chen[b]

[a] *Supercomputing Center, Computer Network Information Center, Chinese Academy of Sciences, P.O. Box 349, Beijing 100080, People's Republic of China*

[b] *Department of Electronic Engineering, City University of Hong Kong, Kowloon, Hong Kong, People's Republic of China*

Received 12 October 2002; accepted 27 March 2003

Abstract

We study the problems of suppressing or inducing chaotic dynamics in a simple model of robot arms and mechanical manipulators, assuming that the unperturbed systems possess multiple non-transverse homoclinic and/or heteroclinic orbits depending on the model parameters. Based on the Melnikov method and numerical computations for Melnikov integrals, fixed points, and turning points, we obtain conditions for chaos suppression and generation. We prove that the initial phase difference Ψ plays an important role in suppressing or inducing chaos in complex systems. Our results indicate that these methods of controlling or inducing chaos can be easily applied to many systems in natural science and engineering.

1. Introduction

Open-loop or non-feedback control techniques for suppressing or preserving chaos have been extensively investigated in recent years [1–8]. In particular, one technique is based on the calculation of the Melnikov function and choosing the control term to destroy or to preserve an inequality that guarantees the existence of a simple zero of the Melnikov function. For systems with two input forces, based on the Melnikov method and numerical simulations, numerous examples have shown that chaotic system dynamics are sensitive to the initial phase difference

*Corresponding author. Present address: Department of Mathematics, School of Science, Beijing Jiaotong University, Beijing 100044, People's Republic of China.

E-mail address: hjcao@center.njtu.edu.cn (H. Cao).

0022-460X/03/$ - see front matter © 2003 Elsevier Ltd. All rights reserved.
doi:10.1016/S0022-460X(03)00382-1

between two forces. Therefore, if one can choose a proper initial phase difference in the parameter space, chaos can be completely eliminated or purposefully created.

However, a number of studies on various dynamical systems by using the aforementioned technique only considered the case where there exists a pair of (or a single) homoclinic (heteroclinic) orbits in a general nonautonomous system, and these homoclinic (heteroclinic) orbits' analytical expressions can be easily obtained, so that the calculation of Melnikov functions (integrals) is easy or at least is possible by using the standard integral tables [9] or complicated residue computations. If a dynamical system possesses multiple saddle points with non-transverse homoclinic and/or heteroclinic orbits, but their analytical expressions of homoclinic and/or heteroclinic orbits of the unperturbed system are impossible to obtain, how to apply this kind of non-feedback control technique to control (suppress or create) chaos?

In this paper, we take the following system as an example to answer the above question

$$\begin{aligned} \dot{x} &= y, \\ \dot{y} &= -\sin x - \alpha x + \beta - \delta y + \gamma \cos(\omega t) + F\gamma \cos(\omega t + \Psi), \end{aligned} \tag{1}$$

where all coefficients and parameters are constants. We introduce a small parameter $\varepsilon \ll 1$ and assume that $\delta, \gamma = O(\varepsilon)$, but $\alpha, \beta, \omega = O(1)$; F is an adjustable parameter, and Ψ is an initial phase difference between the two periodic perturbations $\gamma \cos(\omega t)$ and $F\gamma \cos(\omega t + \Psi)$.

When $F = 0$, the system presents a simple model for robot arms and some mechanical manipulators. There have been a number of experimental [10], theoretical [11,12], and numerical [13] studies of some special case of Eq. (1). Chaotic motions in robot arms have been observed by many researchers in laboratory experiments. In such situations, the arms show irregular and usually violent vibrations. If these vibrations are harmful (often, this is the case), they need to be suppressed. But if they are useful (e.g., used as a mixer of different liquids, chemicals, or powders), they need to be created or enhanced.

When $\delta = 0$, $\gamma = 0$, Eq. (1) becomes a planar Hamiltonian system, which possesses multiple non-transverse homoclinic and/or heteroclinic orbits. Very complicated dynamics are expected to occur. For a similar case to Eq. (1), Li and Moon [14] studied the chaotic dynamics of two well-potential systems with multiple homoclinic and heteroclinic orbits.

The purpose of this paper is mainly to present some feasible computational controllability (suppressing or inducing) conditions of chaos for the complex system (1), assuming that the unperturbed system possesses multiple non-transverse homoclinic and/or heteroclinic orbits.

The paper is organized as follows. In Section 2, we present some numerical results concerning two cases of non-transverse homoclinic and heteroclinic motions including fixed points and turning points in the unperturbed system. In Section 3, the Melnikov analysis is performed for Eq. (1), and criteria for the existence and non-existence of chaos are derived. In addition, n this section, to study the effect of adding the second periodic perturbation, we discuss occurrence of chaotic motions for $F = 0$. Section 4 develops an algorithms for Melnikov integrals for two cases. Compared with a classical example, two results performed by analytical computation and numerical computation are given in Section 5. Suppression (or inducing) conditions for chaos are deduced from Melnikov method, and analytical prediction

of chaos is proved with numerical simulations in Section 6. Finally, conclusions are given in Section 7.

2. Numerical results concerning two cases in the unperturbed systems

When $\gamma = 0$ and $\delta = 0$, Eq. (1) becomes

$$\begin{aligned} \dot{x} &= y, \\ \dot{y} &= -\sin x - \alpha x + \beta. \end{aligned} \tag{2}$$

Eq. (2) is an unperturbed system with a Hamiltonian function

$$H(x, y) = \tfrac{1}{2} y^2 - \cos x + \tfrac{1}{2} \alpha x^2 - \beta x. \tag{3}$$

Eq. (3) has degenerate homoclinic and heteroclinic orbits in some regions of the parameter space (α, β). Figs. 1 and 2 show homoclinic and heteroclinic orbits for two pairs of α and β, respectively. It is shown that there exist a pair of homoclinic orbits $\{q_i^{\pm}(t) | t \in \mathbf{R}\}$ corresponding to the parameters $(\alpha = 0.5, \beta = 1.6)$ in Fig. 1, in which the "+" stands for the right homoclinic orbit, and the "−" denotes the left one. There exist a pair of homoclinic orbits $\{q_i^{-}(t) | t \in \mathbf{R}\}$, $\{q_j^{+}(t) | t \in \mathbf{R}\}$, a pair of heteroclinic orbits $\{q_{ij}(t) | t \in \mathbf{R}\}$, with $\{q_{ji}(t) | t \in \mathbf{R}\}$ corresponding to the parameters $(\alpha = 0.15, \beta = 0)$ in Fig. 2, in which the "*ij*" means that the direction of the heteroclinic orbit is from x_i to x_j, and "*ji*" is from x_j to x_i. Thus, the phase space of Eq. (3) has a great variety of dynamics depending on the parameters α and β.

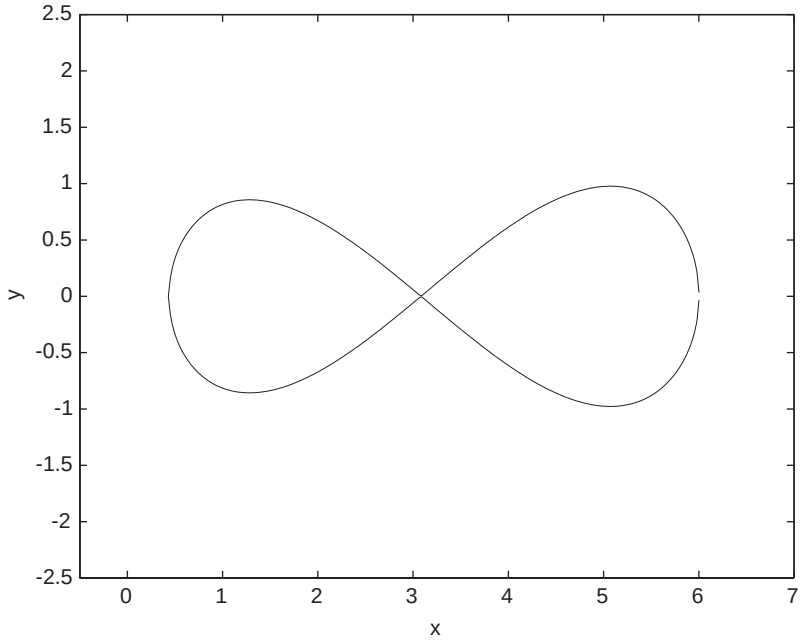

Fig. 1. Homoclinic orbits of equation (2): $\alpha = 0.5$, $\beta = 1.6$.

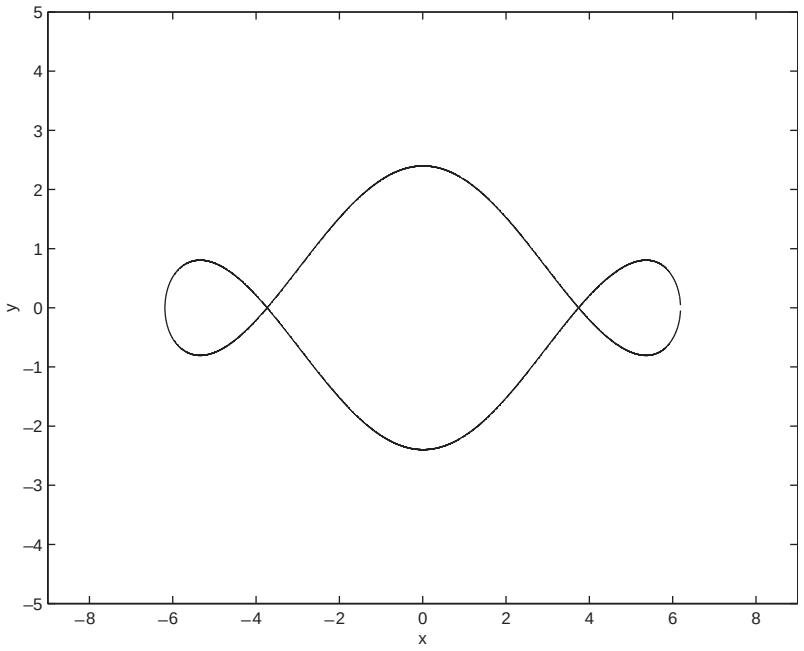

Fig. 2. Heteroclinic orbits of equation (2): $\alpha = 0.15$, $\beta = 0$.

Table 1
The saddle points and turning points of the unperturbed system (2)

PV	Left TP x_i^-	First SP x_i	Second SP x_j	Right TP x_i^+ or x_j^+	HF
$(\alpha = 0.5, \beta = 1.6)$	0.4379	3.0831		6.0017	−3.1166
$(\alpha = 0.15, \beta = 0)$	−6.1867	−3.7366	3.7366	6.1867	3.7506

The fixed points and turning points of the unperturbed system (2) satisfy the following two equations, respectively

$$\begin{aligned} &-\sin(x) - \alpha x + \beta = 0, \\ &2H + 2\cos(x) - \alpha x^2 + 2\beta x = 0, \end{aligned} \tag{4}$$

where H denotes the Hamiltonian function at the fixed points.

The fixed points and the turning points of unperturbed system (2) are obtained by numerically solving Eq. (4) using for instance the bisection method. After the numerical computation, corresponding to the two cases in Figs. 1 and 2, respectively, the parameter values (PV), the saddle point(s) (SP), the turning points (TP), and the Hamiltonian function (HF) are obtained as shown in Table 1.

From Figs. 1 and 2, it can be seen that each saddle has homoclinic and/or heteroclinic orbits, which are contained in the level set determined by Eq. (3). Unfortunately, we do not have

analytical expressions for these homoclinic and heteroclinic orbits; therefore, numerical approach is necessary.

3. Chaotic motion by an additional periodic perturbation

3.1. The existence of chaos for case $F = 0$: numerical results

Before we go on to study the effect by adding the second periodic perturbation, we briefly discuss the occurrence of chaotic motions for $F = 0$. More detailed results can be found in Ref. [12]. We fix (i) $\alpha = 0.5$, $\beta = 1.6$, $\delta = 0.12$, $\omega = 0.75$, and the existence of chaotic motions beyond the Melnikov analytical threshold value γ_c is 0.3 for this case; (ii) $\alpha = 0.15$, $\beta = 0$, $\delta = 0.12$, $\omega = 0.75$, and the existence of chaotic motions beyond the Melnikov analytical threshold value γ_c is 0.7 for this case.

For clarity, the chaotic orbit in the phase space, the (x, y)-plane, and the strange attractor in the Poincaré map for two cases, are given in Figs. 3–6.

We next study the effect of the second periodic perturbation on chaotic motions observed for Cases 1 and 2.

3.2. The existence of chaos for case $F \neq 0$: Melnikov analysis

Here, we apply Melnikov method to Eq. (2) and obtain criteria for suppression of chaos.

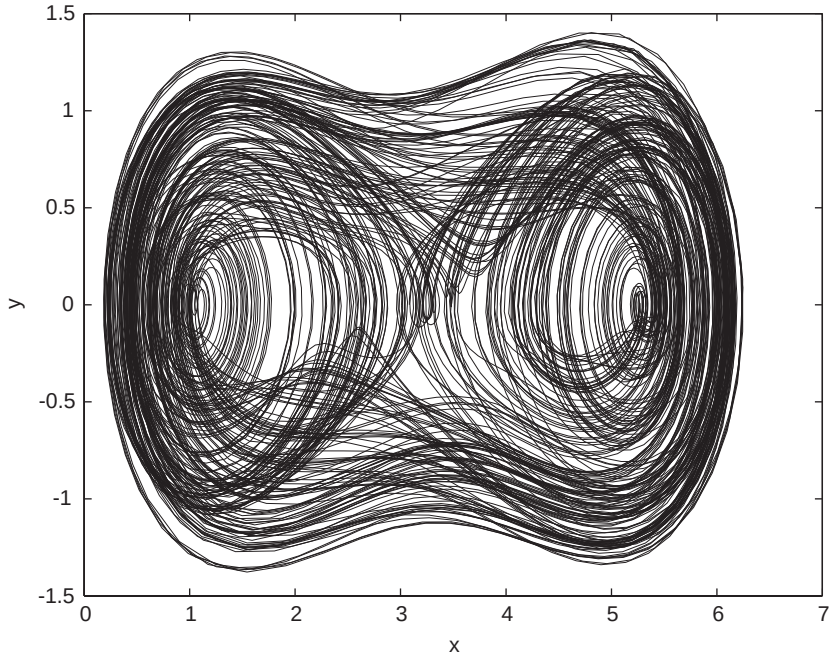

Fig. 3. Phase portrait for Case 1: $\gamma = 0.3$.

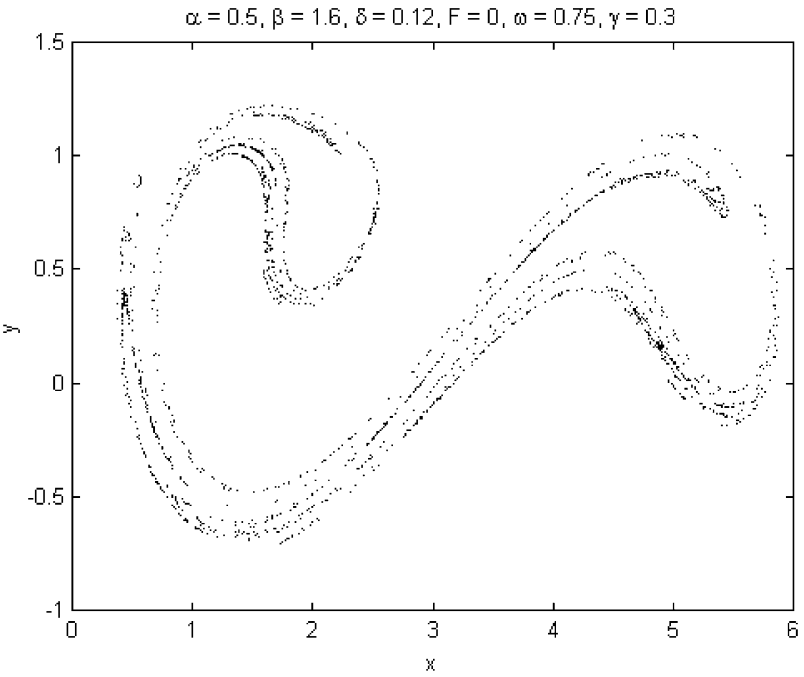

Fig. 4. Poincaré map of the chaotic attractor for $\gamma = 0.3$ in Case 1.

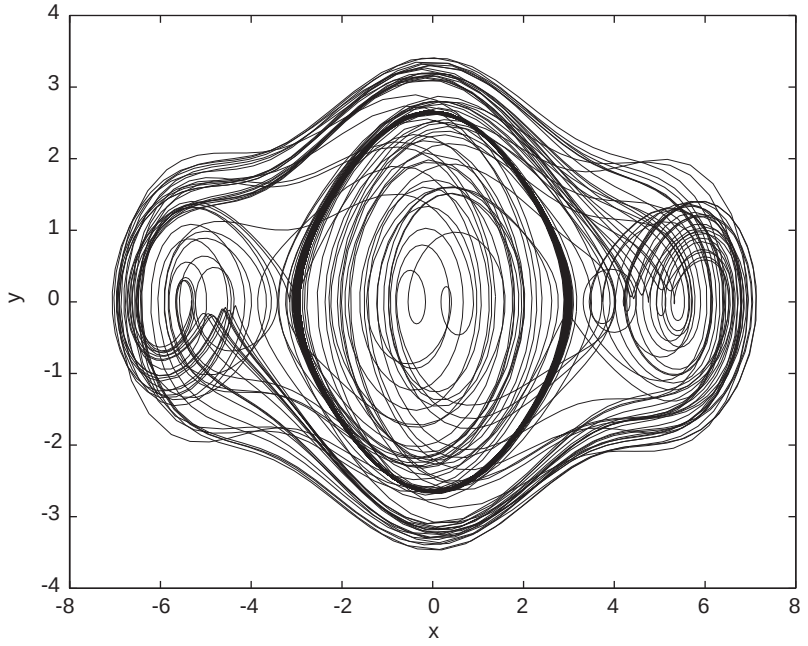

Fig. 5. Phase portrait for Case 2: $\gamma = 0.7$.

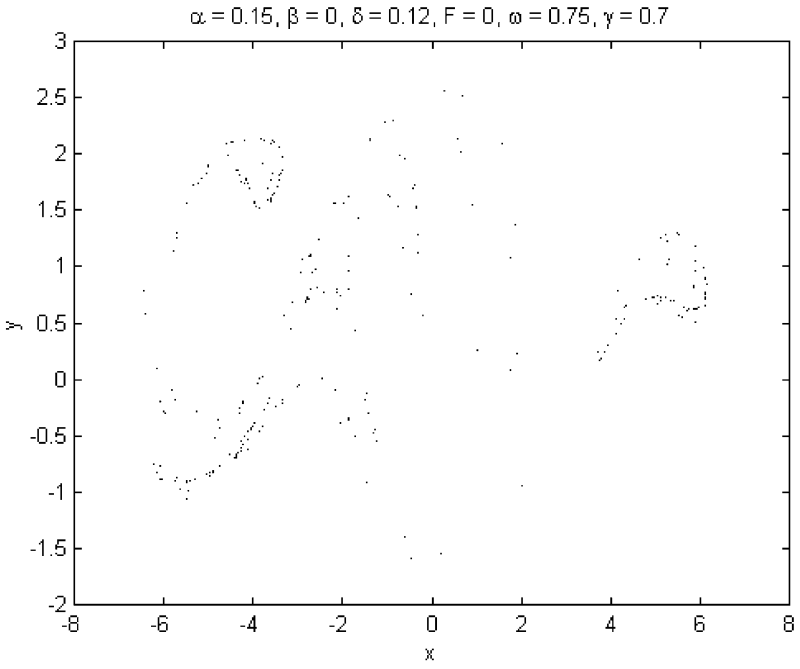

Fig. 6. Poincaré map of the chaotic attractor for $\gamma = 0.7$ in Case 2.

When $\gamma \neq 0$ and $\delta \neq 0$ are small enough, Eq. (1) may have "transverse" homoclinic and heteroclinic orbits. By the Smale–Birkhoff homoclinic theorem [15–17], the existence of such orbits may result in chaotic dynamics. Melnikov's method is an analytical technique for detecting the occurrence of this type of chaotic dynamics and has been successfully applied to several systems containing multiple saddle fixed points.

We first consider the case shown in Fig. 1. The distance between the stable manifold and unstable manifold can be measured by the Melnikov functions $M_i^{\pm}(t_0)$, and in the following we denote the homoclinic orbits of the unperturbed system as $\{q_i^{\pm}(t) | t \in \mathbf{R}\} = (x_i^{\pm}(t), y_i^{\pm}(t))$. We can chose proper initial conditions for these homoclinic orbits such that $y_i^{\pm}(t)$ is an odd function of t.

The Melnikov function can be calculated as follows:

$$\begin{aligned} M_i^{\pm}(t_0) &= \int_{-\infty}^{\infty} y_i^{\pm}(t)[-\delta y_i^{\pm}(t) + \gamma \cos \omega(t + t_0) + F\gamma \cos(\omega(t + t_0) + \Psi)]\,\mathrm{d}t \\ &= -\delta \int_{-\infty}^{\infty} [y_i^{\pm}(t)]^2\,\mathrm{d}t - \left[\gamma(1 + F\cos(\Psi)) \int_{-\infty}^{\infty} y_i^{\pm}(t) \sin(\omega t)\,\mathrm{d}t\right] \sin(\omega t_0) \\ &\quad - \left[F\gamma \sin(\Psi) \int_{-\infty}^{\infty} y_i^{\pm}(t) \sin(\omega t)\,\mathrm{d}t\right] \cos(\omega t_0) \\ &= -\delta B_i^{\pm} - [\gamma(1 + F\cos(\Psi))A_i^{\pm}] \sin(\omega t_0) - [F\gamma \sin(\Psi)A_i^{\pm}] \cos(\omega t_0) \\ &= -\delta B_i^{\pm} - \gamma A_i^{\pm}(\sqrt{F^2 + 2\cos(\Psi)F + 1}) \sin(\omega t_0 + \Theta_i^{\pm}), \end{aligned} \tag{5}$$

where

$$A_i^{\pm} = \int_{-\infty}^{\infty} y_i^{\pm}(t)\sin(\omega t)\,\mathrm{d}t,$$
$$B_i^{\pm} = \int_{-\infty}^{\infty} [y_i^{\pm}(t)]^2\,\mathrm{d}t,$$
$$\Theta_i^{\pm} = \arctan\left(\frac{1+F\cos(\Psi)}{F\sin(\Psi)}\right),$$

and the positive (negative) sign refers to the left (right) homoclinic orbit.

It follows from the Melnikov theory that the condition for $M^{\pm}(t_0)$ to change sign is

$$\delta|B_i^{\pm}| \leqslant \gamma|A_i^{\pm}|\sqrt{F^2+2\cos(\Psi)F+1}, \tag{6}$$

that is,

$$F^2+2\cos(\Psi)F+1-\left(\frac{\delta|B_i^{\pm}|}{\gamma|A_i^{\pm}|}\right)^2 \geqslant 0, \tag{7}$$

where the equal sign corresponds to the case of tangency between the stable and unstable manifolds.

Conversely, if we let

$$F^2+2\cos(\Psi)F+1-\left(\frac{\delta|B_i^{\pm}|}{\gamma|A_i^{\pm}|}\right)^2 < 0, \tag{8}$$

then this inequality provides a necessary condition for $M_i^{\pm}(t_0)$ not to change sign. This condition is also sufficient to assure that $M_i^{\pm}(t_0)$ will not change sign under the main resonant condition. So, we can deduce a wide range for the initial phase difference Ψ from condition (8).

We next consider Case 2 shown in Fig. 2, in which there exist two heteroclinic orbits, $q_{ij}(t) = (x_{ij}(t), y_{ij}(t))$, $q_{ji}(t) = (x_{ji}(t), y_{ji}(t))$, two homoclinic orbits, $q_i^-(t) = (x_i^-(t), y_i^-(t))$ and $q_j^+(t) = (x_j^+(t), y_j^+(t))$, associated with the hyperbolic fixed points p_i and p_j.

The Melnikov function $M_{ij}(t_0)$ for $q_{ij}(t)$ is given by

$$\begin{aligned} M_{ij}(t_0) &= \int_{-\infty}^{\infty} y_{ij}(t)[-\delta y_{ij}(t)+\gamma\cos\omega(t+t_0)+F\gamma\cos(\omega(t+t_0)+\Psi)]\,\mathrm{d}t \\ &= -\delta B_{ij}+[\gamma(1+F\cos(\Psi)C_{ij}-F\gamma\sin(\Psi)S_{ij}]\cos(\omega t_0) \\ &\quad -[\gamma(1+F\cos(\Psi))S_{ij}+F\gamma\sin(\Psi)C_{ij}]\sin(\omega t_0) \\ &= -\delta B_{ij}+\gamma A_{ij}\sqrt{F^2+2\cos(\Psi)F+1}\cos(\omega t_0+\Theta_{ij}), \end{aligned} \tag{9}$$

where

$$C_{ij} = \int_{-\infty}^{\infty} y_{ij}(t)\cos(\omega t)\,\mathrm{d}t,$$
$$S_{ij} = \int_{-\infty}^{\infty} y_{ij}(t)\sin(\omega t)\,\mathrm{d}t, \tag{10}$$

and

$$A_{ij} = \sqrt{C_{ij}^2 + S_{ij}^2},$$
$$B_{ij} = \int_{-\infty}^{\infty} [y_{ij}(t)]^2 \, \mathrm{d}t,$$
$$\Theta_{ij} = \arctan\left(\frac{(1 + F\cos(\Psi))S_{ij} + F\sin(\Psi)C_{ij}}{(1 + F\cos(\Psi)C_{ij} - F\sin(\Psi)S_{ij}}\right). \tag{11}$$

Similarly, the Melnikov function $M_{ji}(t_0)$ for $q_{ji}(t)$ becomes

$$M_{ji}(t_0) = -\delta B_{ij} - \gamma A_{ij}\sqrt{F^2 + 2\cos(\Psi)F + 1}\cos(\omega t_0 + \Theta_{ij}), \tag{12}$$

where we have used the following symmetry equations

$$x_{ij}(t) = x_{ji}(-t), \quad y_{ij}(t) = -y_{ji}(-t). \tag{13}$$

For the left homoclinic orbit $q_i^-(t) = (x_i^-(t), y_i^-(t))$ and the right homoclinic one $q_j^+(t) = (x_j^+(t), y_j^+(t))$, the corresponding Melnikov functions are the following

$$M_i^-(t_0) = -\delta B_i^- - \gamma A_i^-(\sqrt{F^2 + 2\cos(\Psi)F + 1})\sin(\omega t_0 + \Theta_i^-) \tag{14}$$

and

$$M_j^+(t_0) = -\delta B_j^+ - \gamma A_j^+(\sqrt{F^2 + 2\cos(\Psi)F + 1})\sin(\omega t_0 + \Theta_j^+), \tag{15}$$

where the corresponding coefficients are similar to those in the first case.

It follows from the Melnikov theory that the condition for $M_{ij}(t_0)$ to change sign is

$$\delta|B_{ij}| \leqslant \gamma|A_{ij}|\sqrt{F^2 + 2\cos(\Psi)F + 1}, \tag{16}$$

that is,

$$F^2 + 2\cos(\Psi)F + 1 - \left(\frac{\delta|B_{ij}|}{\gamma|A_{ij}|}\right)^2 \geqslant 0. \tag{17}$$

Then, the Melnikov functions $M_{ij}(t_0)$ and $M_{ji}(t_0)$ have simple zeros, and the stable manifolds and unstable manifolds intersect transversely. Here, the equal sign corresponds to the case of tangency between the stable and unstable manifolds.

Conversely, if we let

$$F^2 + 2\cos(\Psi)F + 1 - \left(\frac{\delta|B_{ij}|}{\gamma|A_{ij}|}\right)^2 < 0, \tag{18}$$

then this condition provides a necessary condition for $M_{ij}(t_0)$ and $M_{ji}(t_0)$ not to change sign. These condition are also sufficient to assure that $M_{ij}(t_0)$ and $M_{ji}(t_0)$ will not change sign under the main resonant conditions. So, we can deduce a wide range for the initial phase difference Ψ from condition (18).

For the left (right) homoclinic orbits, we have similar results.

Hence, according to the Smale–Birkhoff homoclinic theorem, chaotic dynamics may occur in the system described by Eq. (1), not only the stable manifolds and unstable manifolds of homoclinic orbits intersect transversely but also the stable manifolds and unstable manifolds of heteroclinic orbits intersect transversely, which lead to very complicated dynamics.

4. Numerical computation of Melnikov integrals

From Section 3, we see that it is very important to compute the Melnikov integrals so as to verify the derived criteria. However, analytical expressions for the unperturbed homoclinic and heteroclinic orbits cannot be obtained. So numerical computations of the integrals are necessary. Here, we adopt the method performed by Bruhn and Koch [11] and Yagasaki [13]. Our main algorithm is based on the fact that the time variable t can be written as functions of the state variable x on homoclinic and heteroclinic orbits. In doing so, the computation of Melnikov integrals can be transformed from that for the time variable t into that for the state variable x.

We first consider the case of homoclinic orbits $\{q_i^{\pm}(t)\}$. From Eqs. (2) and (3), we have

$$\frac{\mathrm{d}x}{\mathrm{d}t} = \mp\sqrt{2H_i + 2\cos x - \alpha x^2 + 2\beta x}, \tag{19}$$

on the homoclinic orbits $\{q_i^{\pm}(t)\}$ for $t > 0$. Let $\bar{x}_i^{\pm}$ be solutions of the transcendent equation

$$-2\cos x + \alpha x^2 - 2\beta x = 2H_i, \tag{20}$$

such that $\bar{x}_i^- < \bar{x}_i^+$. The points $(\bar{x}_i^{\pm}, 0)$ are turning points of the homoclinic orbits. Integrating Eq. (19) yields

$$t = \mp\int_{\bar{x}_i^{\pm}}^{x} \frac{\mathrm{d}\xi}{\sqrt{2H_i + 2\cos\xi - \alpha\xi^2 + 2\beta\xi}}. \tag{21}$$

Substituting Eq. (21) into Eq. (5), we obtain

$$\begin{aligned} A_i^{\pm} &= \mp 2\int_{\bar{x}_i^{\pm}}^{x_i} \sin\left(\omega\int_{\bar{x}_i^{\pm}}^{x} \frac{\mathrm{d}\xi}{\sqrt{2H_i + 2\cos\xi - \alpha\xi^2 + 2\beta\xi}}\right)\mathrm{d}x, \\ B_i^{\pm} &= \mp 2\int_{\bar{x}_i^{\pm}}^{x_i} \sqrt{2H_i + 2\cos\xi - \alpha\xi^2 + 2\beta\xi}\,\mathrm{d}x. \end{aligned} \tag{22}$$

Hence, we can numerically estimate condition (8) as follows. At first the fixed point x_i and the turning points $\bar{x}_i^{\pm}$ are obtained by numerically solving Eqs. (2) and (3) using the bisection method. We then numerically estimate the definite integrals $A_i^{\pm}$ and $B_i^{\pm}$ given by Eq. (5) using Simpson's rule. The integration of $A_i^{\pm}$ is performed by changing the upper and lower limits of integration from x_i to $x_i \pm \Delta x$ and $\bar{x}_i^{\pm} \mp \Delta x$, where Δx is a small positive constant, since the integrands are singular near these points.

We next consider the case shown in Fig. 2. We can assume that $x_i < x_j$ without loss of generality. By noting that Eq. (21) also holds on heteroclinic orbits, the second equation of Eq. (11) can be written as

$$B_{ij} = \int_{x_i}^{x_j} \sqrt{2H_i + 2\cos x - \alpha x^2 + 2\beta x}\,\mathrm{d}x. \tag{23}$$

As in the homoclinic case, we have

$$t = \int_{x_{ij}(0)}^{x} \frac{\mathrm{d}\xi}{\sqrt{2H_i + 2\cos\xi - \alpha\xi^2 + 2\beta\xi}} \tag{24}$$

on the heteroclinic orbit $q_{ij}(t)$. Substituting Eq. (24) into Eq. (10) yields

$$C_{ij} = \int_{x_i}^{x_j} \cos\left(\omega \int_{x_{ij}(0)}^{x} \frac{\mathrm{d}\xi}{\sqrt{2H_i + 2\cos\xi - \alpha\xi^2 + 2\beta\xi}}\right) \mathrm{d}x,$$

$$S_{ij} = \int_{x_i}^{x_j} \sin\left(\omega \int_{x_{ij}(0)}^{x} \frac{\mathrm{d}\xi}{\sqrt{2H_i + 2\cos\xi - \alpha\xi^2 + 2\beta\xi}}\right) \mathrm{d}x. \tag{25}$$

The fixed points x_i and x_j are obtained by numerically solving Eqs. (2) and (3), and the definite integrals B_{ij}, C_{ij} and S_{ij} in Eq. (25) are then numerically estimated. The limits of integration are, if necessary, changed from x_i and x_j to $x_i + \Delta x$ and $x_j - \Delta x$ (with small $\Delta x > 0$), respectively.

5. Compared with the analytical algorithm

In this section, to verify whether there exists a relatively good agreement between the numerical algorithm and the analytical one, we use the following system as an example

$$\begin{aligned} \dot{x} &= y, \\ \dot{y} &= -\sin x + \varepsilon[(\alpha - \beta y^2)y + \gamma\cos(\omega t)], \end{aligned} \tag{26}$$

where ε is small perturbation parameter.

When $\varepsilon = 0$, Eq. (26) is an Hamiltonian system with heteroclinic orbits given by analytical expressions as follows

$$x_{ij}(t) = \pm 2\arctan(\mathrm{e}^t), \quad y_{ij}(t) = \pm 2\,\mathrm{sech}(t). \tag{27}$$

In addition, there exist one center, $(0, 0)$, and two saddle points, $(-\pi, 0)$, $(\pi, 0)$.

For Eq. (26), Litak et al. [18] gave some detailed analysis for its chaotic motion by means of combing Melnikov analysis and numerical methods.

The Melnikov function for this system is given by

$$M_{ij}(t_0) = \int_{-\infty}^{\infty} (\alpha - \beta y_{ij}^2(t)) y_{ij}^2(t)\,\mathrm{d}t + \gamma \int_{-\infty}^{\infty} y_{ij}(t)\cos[\omega(t + t_0)]\,\mathrm{d}t, \tag{28}$$

where the positive (negative) sign refers to the top (bottom) heteroclinic orbit.

Substituting Eq. (27) into Eq. (28), the Melnikov function works out to be

$$M_{ij}(t_0) = -B_{ij} \pm A_{ij}\cos(\omega t_0), \tag{29}$$

with

$$B_{ij} = 8\alpha - \tfrac{64}{3}\beta,$$
$$A_{ij} = 2\pi\gamma \operatorname{sech}\left(\frac{\pi\omega}{2}\right). \tag{30}$$

Thus, the critical amplitude of the external forcing, for which the heteroclinic bifurcation occurs, is as follows

$$\gamma_c = \frac{4}{\pi}\left|\alpha - \frac{8}{3}\beta\right| \cosh\left(\frac{\omega}{2}\right). \tag{31}$$

Then, we can directly use the analytical expression (31) to plot the homoclinic bifurcation curve.

In the following, we present the numerical results by using the algorithm developed in Section 4.

First, from the Hamiltonian function $H = y^2/2 - \cos(x)$ and the first equation of Eq. (26), we obtain the time variable t as follows:

$$t = \mp \int_{\pi}^{x} \frac{\mathrm{d}\xi}{\sqrt{2H + 2\cos(\xi)}}.$$

Second, using the equality $y\,\mathrm{d}t = \mathrm{d}x$, Eq. (28) can be written as

$$M_{ij}(t_0) = B_{ij} + \gamma A_{ij} \cos(\omega t_0 + \Theta_{ij}), \tag{32}$$

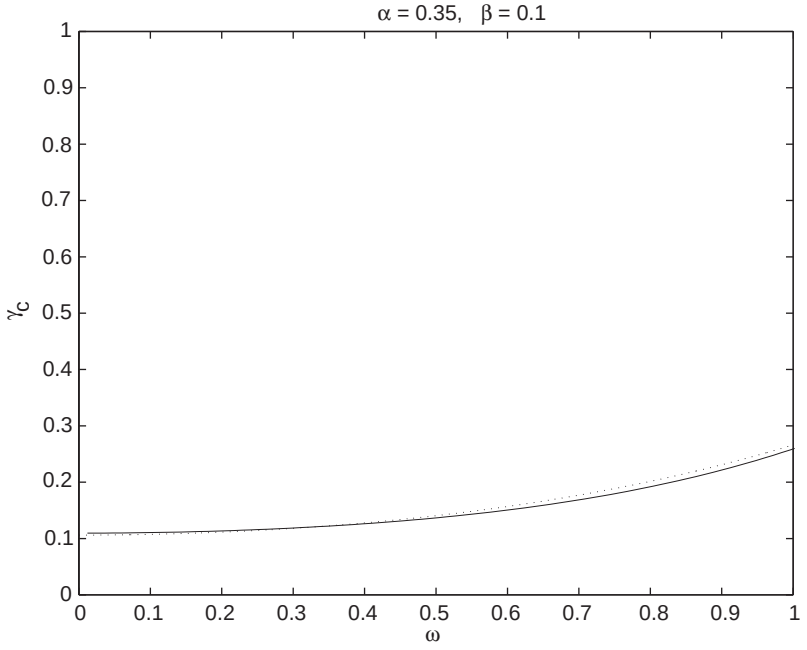

Fig. 7. Heteroclinic bifurcation curves computed by two algorithms: the solid line was computed by the developed numerical algorithm; while the dotted line was computed by the analytical expression (31).

where

$$B_{ij} = \alpha \int_{-\pi}^{\pi} y \, \mathrm{d}x - \beta \int_{-\pi}^{\pi} y^3 \, \mathrm{d}x,$$
$$C_{ij} = \int_{-\pi}^{\pi} \cos\left(\omega \int_{-\pi}^{x} \frac{\mathrm{d}\xi}{\sqrt{2H + 2\cos\xi}}\right) \mathrm{d}x,$$
$$S_{ij} = \int_{-\pi}^{\pi} \sin\left(\omega \int_{-\pi}^{x} \frac{\mathrm{d}\xi}{\sqrt{2H + 2\cos\xi}}\right) \mathrm{d}x,$$
$$A_{ij} = \sqrt{C_{ij}^2 + S_{ij}^2}. \tag{33}$$

Finally, using Simpson's rule, B_{ij} and A_{ij} can be obtained with 800 steps for integration about ξ and with 400 steps for integration about x in the range of the forced frequency $\omega \in [0, 1]$.

Using the developed numerical algorithm and analytical expression (31), respectively, we plot two heteroclinic bifurcation curves in Fig. 7, in which the solid line is the heteroclinic bifurcation curve computed by numerical algorithm, while the dotted line denotes the heteroclinic bifurcation curve performed by the analytical expression (31). It can be seen that the two results are in good agreement.

6. Suppressing or inducing chaos by Melnikov method: numerical results

We first present numerical results for the first case.

Substituting $A_i^{\pm}$ and $B_i^{\pm}$ into the right-hand side of inequality (8), and setting the inequality be zero, we have

$$F^2 + 2\cos\Psi F + 1 - \left(\frac{\delta B_i^{\pm}}{\gamma A_i^{\pm}}\right)^2 = 0. \tag{34}$$

For Eq. (34), we have the following homoclinic condition for chaos suppression:

Theorem 1. *If* $|\sin\Psi| \leqslant \delta B_i^{\pm}/\gamma A_i^{\pm}$ *and* $F_{min} \leqslant F \leqslant F_{max}$, *then* $M_i^{\pm}(t_0)$ *always has the same sign and consequently no chaotic motions occur in the parameter regions enclosed by the following two curves*:

$$F_{min} = -\cos(\Psi) - \sqrt{\left(\frac{\delta B_i^{\pm}}{\gamma A_i^{\pm}}\right)^2 - (\sin(\Psi))^2}. \tag{35}$$

$$F_{max} = -\cos(\Psi) + \sqrt{\left(\frac{\delta B_i^{\pm}}{\gamma A_i^{\pm}}\right)^2 - (\sin(\Psi))^2}. \tag{36}$$

We set the parameter values as $\alpha = 0.5$, $\beta = 1.6$, $\delta = 0.12$, $\omega = 0.75$, $\gamma = 0.3$, and the F and Ψ are free parameters. First, using the algorithm developed in Section 3, we obtained the value of Melnikov integrals as shown in Table 2, where numerical computations described in Section 3

Table 2
Values of $A_i^{\pm}$ and $B_i^{\pm}$ for Case 1

A_i^+	B_i^+	A_i^-	B_i^-
1.6736	1.9205	1.5131	1.5317

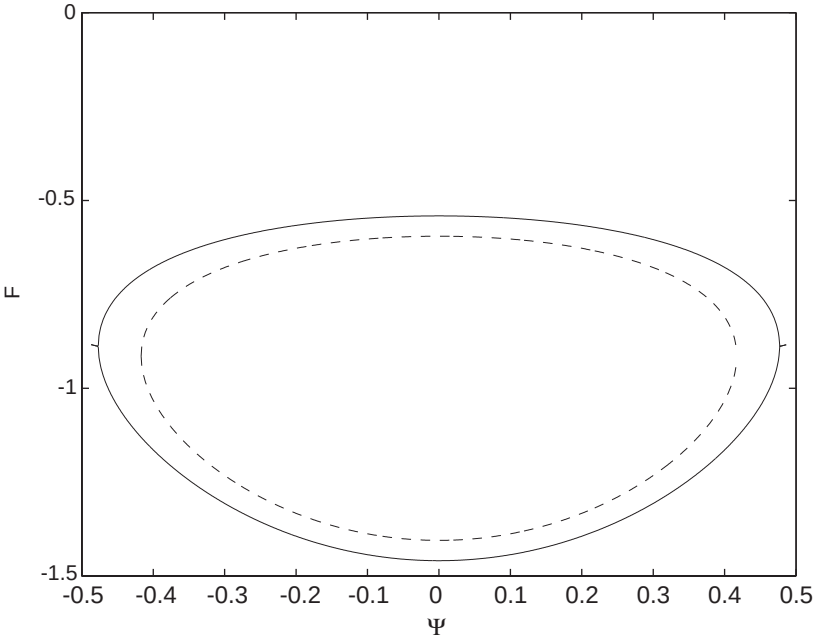

Fig. 8. Chaos does not occur in the region, in which the parameter values are $\alpha = 0.5$, $\beta = 1.6$, $\delta = 0.12$, $\omega = 0.75$, $\gamma = 0.3$.

were performed by setting $\Delta x = 1 \times 10^{-5}$ and using Simpson's rule with 800 steps for integration about ξ and 400 steps for integration about x in Eq. (22).

From the homoclinic suppressing condition and the above Melnikov integral values, we obtain the range of initial phase difference Ψ to be $[-0.476869, 0.476869]$ for the right homoclinic orbit, and $[-0.416891, 0.416891]$ for the left homoclinic orbit. From Eqs. (35) and (36), we note that $M_i^{\pm}(t_0)$ change signs, that is, the transverse intersections of homoclinic orbits occur above and below the curves given by Eqs. (36) and (35), respectively. In the parametric regions enclosed by the two curves, $M_i^{\pm}(t_0)$ does not change sign and hence transverse intersection of homoclinic orbits do not occur. In addition, the parametric regions enclosed by the curves obtained from $M_i^-(t_0)$ is a subregion of the parametric regions enclosed by the curves obtained from $M_i^+(t_0)$.

As an example, we fixed the value of Ψ at 0.3. For this choice, from Eqs. (35) and (36), one can expect suppression of chaos for $F \in [-1.3066, -0.6041]$ corresponding to the right homoclinic orbit, while, for the left homoclinic orbit, the chaos suppressing interval could be in $F \in [-1.2321, -0.6785]$. Out of the ranges of the two intervals, chaos may occur.

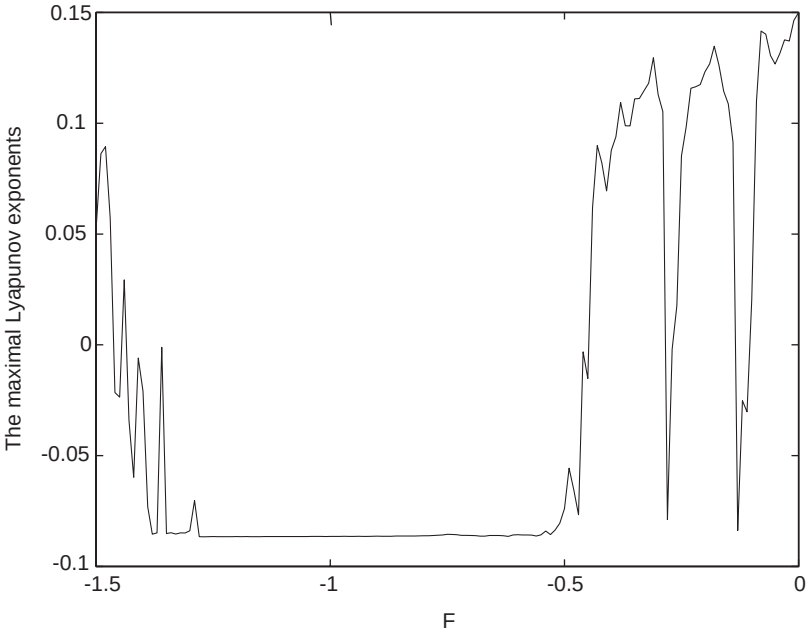

Fig. 9. Maximal Lyapunov exponents. $\alpha = 0.5$, $\beta = 1.6$, $\delta = 0.12$, $\omega = 0.75$, $\gamma = 0.3$, $\Psi = 0.3$.

Fig. 8 shows the two regions, in which the region enclosed by the dashed curve is from the left homoclinic orbit, and the region enclosed by the solid curve is from the right homoclinic orbit.

Fig. 9 shows the maximal Lyapunov exponent λ_1 calculated by Wolf's algorithm [19] versus the second perturbation amplitude F, in which all parameters are fixed except that F varys with increment $\Delta F = 0.001$. When we take the initial phase difference $\Psi = 0.3$, the corresponding maximal Lyapunov exponents are negative for $F \in [-1.4, 0.46]$. It demonstrates that chaotic motion has been suppressed by means of an initial phase difference Ψ in the second weak resonant perturbation term.

Corresponding to the same parameters as that in Fig. 9, we present bifurcation diagrams in Fig. 10. From Fig. 10, it can be seen that the chaotic motion is suppressed if $F \in [-1.4, 0.46]$ and periodic response is obtained in the same interval. If we want to create chaotic motion, we may take the F out of the above interval. For example, when F is in the interval $[-0.47, 0]$, there exist chaotic motions as shown in Fig. 9 corresponding to the positive maximal Lyapunov exponents indicated in Fig. 10.

Similarly, we have the following heteroclinic suppression condition. For the left and right homoclinic orbits, there exist similar results.

Theorem 2. *If* $|\sin\Psi| \leqslant \delta B_{ij}/\gamma A_{ij}$ *and* $F_{min} \leqslant F \leqslant F_{max}$, *then* $M_{ij}(t_0)$ *and* $M_{ji}(t_0)$ *always have the same sign and, consequently, no chaotic motions occur in the parameter regions enclosed by the following*

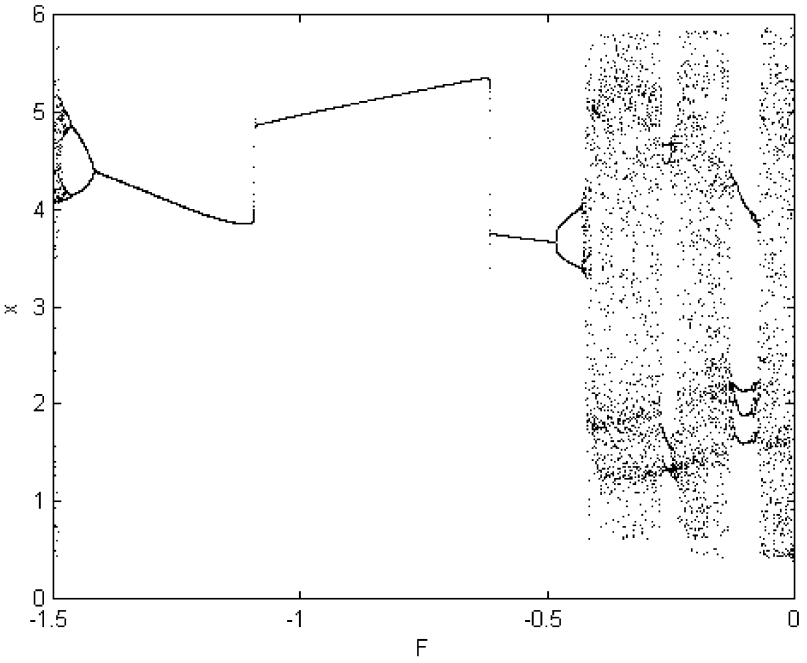

Fig. 10. Bifurcation diagrams for parameter values F ($\Psi = 0.3$). The other parameter values are the same as in Fig. 9.

Table 3
Values of $A_i^{\pm}$, $B_i^{\pm}$, A_{ij}, B_{ij} for Case 2

A_i^-	B_i^-	A_{ij}	B_{ij}	A_i^+	B_i^+
1.4456	1.3583	4.2160	11.0413	1.4456	1.3583

two curves, where

$$F_{min} = -\cos(\Psi) - \sqrt{\left(\frac{\delta B_{ij}}{\gamma A_{ij}}\right)^2 - (\sin(\Psi))^2}. \tag{37}$$

$$F_{max} = -\cos(\Psi) + \sqrt{\left(\frac{\delta B_{ij}}{\gamma A_{ij}}\right)^2 - (\sin(\Psi))^2}. \tag{38}$$

To verify the theoretical results, we set the parameter values as $\alpha = 0.15$, $\beta = 0$, $\delta = 0.12$, $\omega = 0.75$, $\gamma = 0.7$, and F and Ψ are free parameters. First, using the algorithm developed in Section 3, we obtained the Melnikov integrals in Table 3, where numerical computations described in Section 3 were performed by setting $\Delta x = 1 \times 10^{-5}$ and using Simpson's rule with 800 steps for integration about ξ and with 400 steps for integration about x in Eq. (25).

From the suppressing condition and the above Melnikov integral values, we obtain the significant range of initial phase difference Ψ to be $[-0.161779, 0.161779]$ for the left and right homoclinic orbits, and $[-0.465595, 0.465595]$ for the heteroclinic orbits. Obviously, the range of homoclinic orbits is less than the range of heteroclinic orbits. From Eqs. (37) and (38), we note that $M_{ij}(t_0)$ and $M_{ji}(t_0)$ change signs, that is, the transverse intersections of homoclinic orbits or heteroclinic orbits occur above and below the curves given by Eqs. (38) and (37), respectively. In the parametric regions enclosed by the two curves, $M_i^{\pm}(t_0)$ and $M_{ij}(t_0)$ do not change sign and hence transverse intersections of homoclinic orbits and heteroclinic orbits do not occur. In addition, the parametric regions enclosed by the curves obtained from $M_i^{-}(t_0)$ and $M_j^{+}(t_0)$ is a small subregion of the parametric regions enclosed by the curves obtained from $M_{ij}(t_0)$.

As an example, we fixed the value of Ψ at 0.6. For this choice, from Eqs. (37) and (38), one can expect suppressing chaos for $F \in [-1.4860, -0.1647]$, corresponding to the heteroclinic orbit, while there are no significant values for the homoclinic orbits. Out of these ranges of the two intervals, chaos may occur.

We note that the corresponding Melnikov integrals are the same for the left and the right homoclinic orbits due to the symmetry.

Fig. 11 shows the two regions, in which the region enclosed by the dashed curve is from the homoclinic orbits, and the region enclosed by the solid curve is from the heteroclinic orbit. Fig. 12 shows the maximal Lyapunov exponent λ_1 versus the second perturbation amplitude F, in which all parameters are fixed except that F varys with increment $\Delta F = 0.001$. When the initial phase difference $\Psi = 0.6$, the corresponding maximal Lyapunov exponents are negative for $F \in [-1.4, 0.46]$. It demonstrates that chaotic motion has been suppressed by means of an initial phase difference Ψ in the second weak resonant perturbation term.

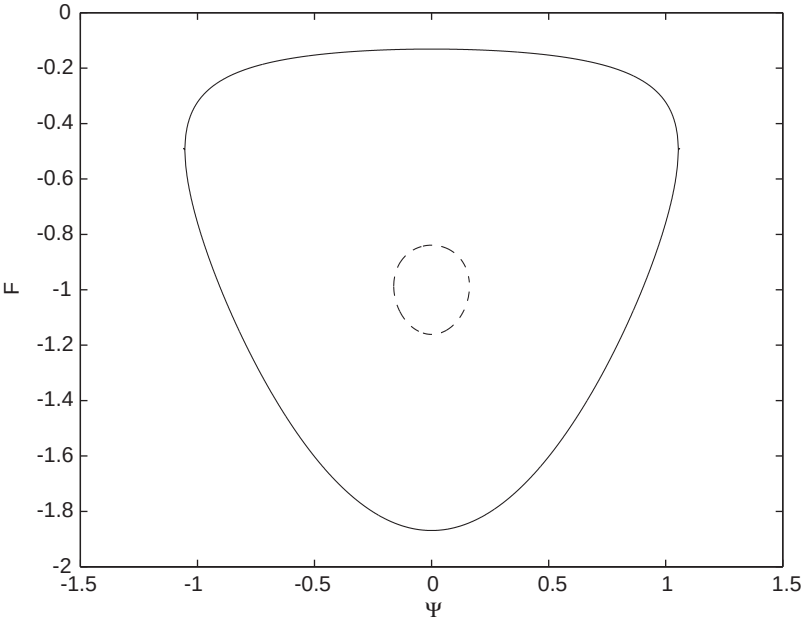

Fig. 11. Chaos does not occur in the region, in which the parameter values are $\alpha = 0.15$, $\beta = 0$, $\delta = 0.12$, $\omega = 0.75$, $\gamma = 0.7$.

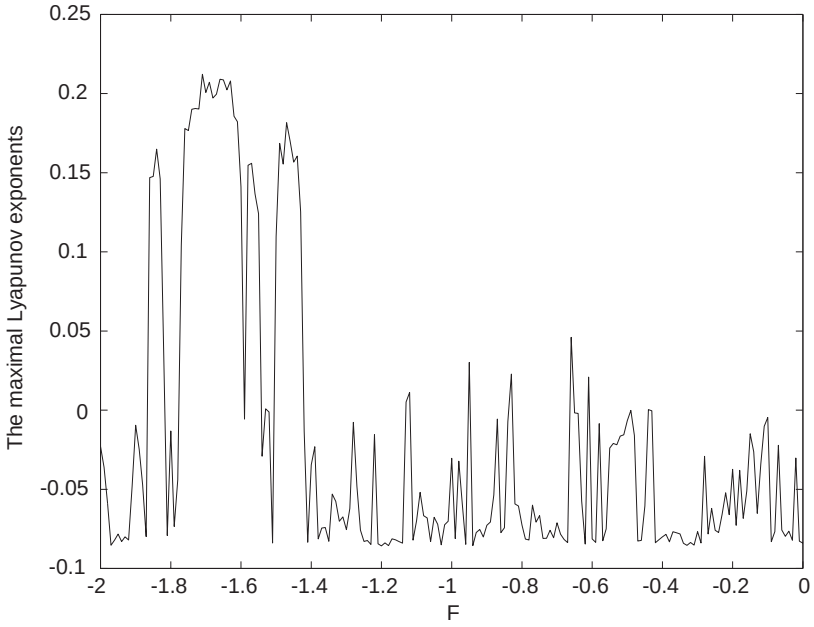

Fig. 12. Maximal Lyapunov exponents. $\alpha = 0.15$, $\beta = 0$, $\delta = 0.12$, $\omega = 0.75$, $\gamma = 0.7$, $\Psi = 0.6$.

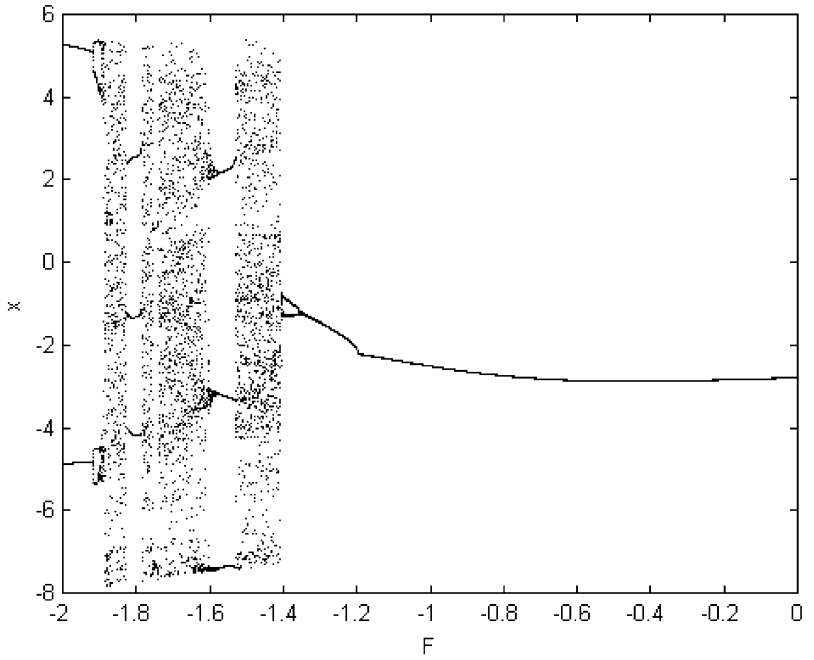

Fig. 13. Bifurcation diagrams for parameter values F ($\Psi = 0.6$). The other parameter values are the same as in Fig. 12.

Corresponding to the same parameters as that in Fig. 12, we present bifurcation diagrams in Fig. 13. From Fig. 13, it can be seen that the chaotic motion is suppressed if $F \in [-1.4, 0.46]$ and periodic response is obtained in the same interval. If we want to create chaotic motion, we may take the F out of the above interval. For example, when F is in the interval $[-1.9, -1.38]$, there exist chaotic motions as shown in Fig. 13 corresponding to the positive maximal Lyapunov exponents indicated in Fig. 12.

7. Conclusions

In this paper, we have studied a rather complicated non-linear dynamical system, for which the unperturbed system possesses multiple non-transverse homoclinic and/or heteroclinic orbits depending on the parameters α and β. For this system, we have presented some conditions for suppressing or inducing chaos by adding a second periodic perturbation and using the initial phase difference as a control term. Based on the Melnikov method and numerical computations for the Melnikov integrals, fixed points, and turning points, we have obtained the controllability regions in the parameter space for chaos suppression or generation. If we choose a proper Ψ, chaos can be completely eliminated or be created as desired.

In practical applications, the second perturbation input, $F\gamma\cos(\omega t + \Psi)$ in Eq. (2), works as an open-loop control input. This signal can be connected directly to the machine through an electronic wire. Physically, an exact signal can be obtained and used by such wiring, without the need of signal identification. Its precise mathematical form is needed only in theoretical analysis, as did in the paper, but not for physical implementation.

There are a number of methods that deal with the chaotic control and chaos generation problems. By comparing the theoretical relevance between the method proposed in this paper and the existing ones, we found that some basic conditions are not comparable, therefore it is difficult to give a correct and fair comparison among different methods. For this reason, we leave a comprehensive comparison study to future studies.

The system considered here shows that there exists different ranges of controlling (suppressing or inducing) chaos in the parameter space for different unperturbed systems. For example, for systems with multiple nontransverse homoclinic orbits, their controlling ranges are almost the same, but for the unperturbed systems with both homoclinic orbits and heteroclinic orbits, their ranges are quite different. Our numerical results have shown that the range affected by heteroclinic orbits is clearly greater than that by homoclinic orbits.

In many fields of natural science and engineering, there are a lot of mathematical models similar to the one we consider here. Therefore, our results of controlling (suppressing or inducing) chaos should be useful for a broad spectrum of applications.

Acknowledgements

This work was partially supported by State Hi-Tech Research and Development Program of China (863) (2002AA104540), the Special Funds for Major State Basic Research Projects of China (G1999032805), and by the Hong Kong Research Grants Council under CERG Grants (CityU

1018/01E and 1004/02E). We are grateful to the reviewers for their helpful suggestions on the original manuscript. We would also like to acknowledge that some of our computations were supported by the Dawning 2000-II supercomputer at the Center for Computer Network Information in the Chinese Academy of Sciences, Beijing, China.

References

[1] A. Lima, M. Pettini, Suppression of chaos by resonant parametric perturbations, Physical Review A 41 (1990) 726–733.
[2] A. Azevedo, S.M. Rezende, Controlling chaos in spin-wave instabilities, Physical Review Letters 66 (1991) 1342–1345.
[3] Y. Braiman, I. Goldhirsch, Taming chaotic dynamics with weak periodic perturbations, Physical Review Letters 66 (1991) 2545–2548.
[4] S. Rajasekar, Controlling of chaos by weak periodic perturbations in Duffing–van der Pol oscillator, Pramana. 41 (1993) 295–309.
[5] Z.R. Liu, Perturbation Criteria for Chaos, Shanghai Scientific and Technological Education Publishing House, Shanghai, 1994 (in Chinese).
[6] G. Chen, X. Dong, From Chaos to Order: Methodologies, Perspectives, and Applications, World Scientific, Singapore, 1998.
[7] R. Chacón, General results on chaos suppression for biharmonically driven dissipative systems, Physical Letters A 257 (1999) 293–300.
[8] R. Chacón, F. Palmero, F. Balibrea, Taming chaos in a driven Josephson junction, International Journal of Bifurcation and chaos 7 (2001) 1897–1909.
[9] I. Gradshteyn, I. Ryzhik, Table of Integrals, Series and Products, Springer, New York, 1994.
[10] K. Yagasaki, A feedback control system: bifurcations of periodic orbits and chaos, Nonlinear Dynamics 9 (1996) 391–417.
[11] B. Bruhn, B.P. Koch, Homoclinic and heteroclinic bifurcations in rf SQUIDs, Zeitschrift für Naturforschung 43a (1988) 930–938.
[12] F.M.A. Salam, S.S. Sasatry, Dynamics of the forced Josephson junction circuit: the region of chaos, IEEE Transactions on Circuits and Systems 32 (1985) 784–796.
[13] K. Yagasaki, Chaos in a pendulum with feedback control, Nonlinear Dynamics 6 (1994) 125–142.
[14] G.X. Li, F.C. Moon, Criteria for chaos of a three-well potential oscillator with homoclinic and heteroclinic orbits, Journal of Sound and Vibration 136 (1990) 17–34.
[15] J. Guckenheimer, P. Holmes, Nonlinear Oscillations, Dynamical Systems, and Bifurcations of Vector Fields, Springer, New York, 1983.
[16] S. Wiggins, Global Bifurcations and Chaos, Springer, New York, 1988.
[17] S. Wiggins, Introduction to Applied Nonlinear Dynamical Systems and Chaos, Springer, New York, 1990.
[18] G. Litak, S. Grzegorz, S. Kazimierz, W. Jerzy, Vibration of externally-forced froude pendulum, Journal of International Bifurcation and Chaos 3 (1999) 561–570.
[19] A. Wolf, J.B. Swift, H.L. Swinney, J.A. Vasano, Determining Lyapunov exponents from a time series, Physica D 16 (1985) 285–317.